Collision Detection and Contact Point Estimation Using Virtual Joint Torque Sensing Applied to a Cobot

Dario Zurlo*, Tom Heitmann†, Merlin Morlock†, and Alessandro De Luca*

***Abstract*— In physical human-robot interaction (pHRI) it is essential to reliably estimate and localize contact forces between the robot and the environment. In this paper, a complete contact detection, isolation, and reaction scheme is presented and tested on a new 6-dof industrial collaborative robot. We combine two popular methods, based on monitoring energy and generalized momentum, to detect and isolate collisions on the whole robot body in a more robust way. The experimental results show the effectiveness of our implementation on the LARA 5 cobot, that only relies on motor current and joint encoder measurements. For validation purposes, contact forces are also measured using an external GTE CoboSafe sensor. After a successful collision detection, the contact point location is isolated using a combination of the residual method based on the generalized momentum with a contact particle filter (CPF) scheme. We show for the first time a successful implementation of such combination on a real robot, without relying on joint torque sensor measurements.**

I. INTRODUCTION

Collaborative robots (cobots) are robots that can be operated in the vicinity of human workers without additional safety installations, such as fences or light barriers. Since cobots can be employed in very dynamic, unstructured and partially unknown environments, where the relative motions between robot and human may be very fast or hardly predictable, it is not always possible to avoid collisions through the usage of external sensors and collision-aware motion planning, as done in [1]. In some cases, the contact is even part of the physical human robot interaction (pHRI). In order to guarantee the safety of the operator, it is essential to be able to detect and isolate contacts with the environment precisely and to be able to react accordingly.

A comprehensive overview of existing techniques is given in [2]. In [3], the authors use contact point and force information in an impedance control scheme. Additionally, precise contact information can be used in grasping scenarios in order to verify the success of the operation. While there exists a variety of methods to estimate the contact forces, most of these methods employ additional sensors. A tactile skin mounted on the robot allows to directly detect contact forces and the contact location, see [4]. Joint torque sensors allow the direct measurement of the mechanical torque acting on each joint without the friction disturbances typically encountered in motor current measurements. Using these

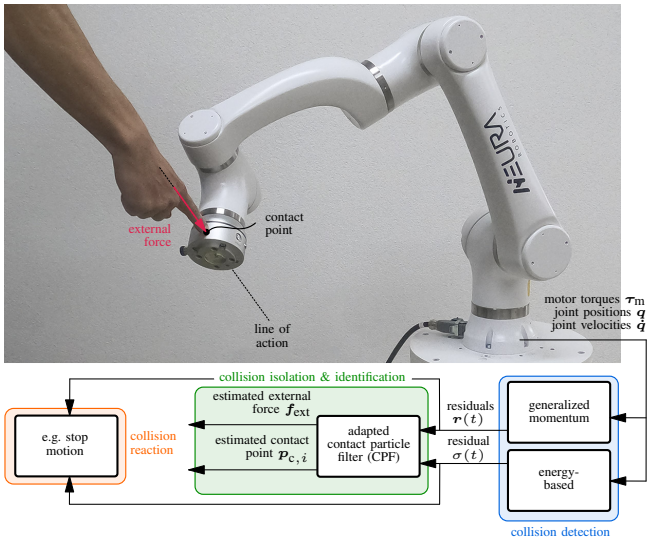

Fig. 1: LARA 5 cobot and proposed collision handling scheme.

sensors with the popular residual method based on the generalized momentum of the robot presented in [5] and [6], it is possible to estimate the contact forces on the robot. This method in combination with joint torque sensors has been successfully applied and experimentally validated on a 7-dof DLR-III robot in [6]. The advantages of using an additional 6-dof force/torque sensor in the robot base are discussed in [7]. Here, the authors show simulatively that it is possible to identify the contact point using only joint torque and encoder measurements via the method of the generalized momentum and a pseudo-inversion of the skew-symmetric matrix that describes the cross product between contact point and contact forces. In [8], the authors show an experimental evaluation of the same method to estimate the contact forces and the contact point on the DLR 7-dof robot SARA using joint torque sensors and two additional 6-dof force/torque sensors, one in the base and one in the wrist. Another popular method for collision detection is based on the energy of the system, see [2].

Instead of computing the contact force and point using the pseudo-inverse method, it is possible to use a contact particle filter (CPF), as presented in [9]. The authors employ the CPF and the residual method on an Atlas humanoid robot in simulation and are able to estimate up to 3 simultaneous contact points accurately. In [10], experimental results of the application of the CPF without the residual method on a KUKA LBR iiwa 7-dof robot are shown, relying only on joint torque sensors and position measurements.

The main contribution of this paper is twofold. First, we combine two existing collision detection methods and

*D. Zurlo and A. De Luca are with the Dipartimento di Ingegneria Informatica, Automatica e Gestionale, Sapienza Università di Roma, Rome, Italy. {zurlo.1676376@studenti, deluca@diag}.uniroma1.it. Financial support from PNRR MUR project PE0000013-FAIR is acknowledged.

†T. Heitmann and M. Morlock are with NEURA Robotics GmbH, Metzingen, Germany.{tom.heitmann, merlin.morlock}@neura-robotics.com.

validate our approach experimentally; second, we propose an adapted CPF scheme for the contact point localization. According to the literature, the contact point estimation based on the residuals of the generalized momentum method without joint torque or any other additional sensors has not yet been realized experimentally. This work shows the experimental application of both the pseudo-inverse and the contact particle filter methods on a 6-dof LARA 5 cobot, relying only on motor current and joint encoder measurements. Further, this work suggests the combination of the two methods by initializing the CPF with the solution of the classical pseudo-inverse method when a contact is detected on link 6.

The paper is organized as follows. Section II introduces the basics of the collision detection method using the energy and generalized momentum of the robot. Section III shows how the classical pseudoinverse method and the CPF can be combined for localizing the contact point. Finally, experimental results are presented in Sec. IV.

II. COLLISION DETECTION

In this section, we introduce the underlying dynamical model of the robot used in this paper, as well as the collision detection method based on the energy of the system [2] and the method based on the generalized momentum [7].

A. Dynamical Model of the Robot

The dynamics of an open-chain serial robot manipulator with n actuated joints are governed by

$$\boldsymbol{M}(\boldsymbol{q})\ddot{\boldsymbol{q}} + \boldsymbol{C}(\boldsymbol{q},\dot{\boldsymbol{q}})\dot{\boldsymbol{q}} + \boldsymbol{g}(\boldsymbol{q}) = \boldsymbol{\tau}_{\text{m}} - \boldsymbol{\tau}_{\text{fric}} + \boldsymbol{\tau}_{\text{ext}}, \quad (1)$$

where $\boldsymbol{q} \in \mathbb{R}^n$ are the generalized (joint) coordinates, $\boldsymbol{M}(\boldsymbol{q}) \in \mathbb{R}^{n\times n}$ is the positive definite inertia matrix of the multi-body system, $\boldsymbol{C}(\boldsymbol{q},\dot{\boldsymbol{q}})\dot{\boldsymbol{q}} \in \mathbb{R}^n$ collects Coriolis and centrifugal forces (quadratic in $\dot{\boldsymbol{q}}$), and $\boldsymbol{g}(\boldsymbol{q}) \in \mathbb{R}^n$ contains the gravitational terms. The motor torques as system inputs are denoted by $\boldsymbol{\tau}_{\text{m}} = \boldsymbol{K}_{\text{i}}\boldsymbol{i}_{\text{m}} \in \mathbb{R}^n$, where $\boldsymbol{K}_{\text{i}}$ is a diagonal matrix containing the motor constants, which scale the measured motor currents $\boldsymbol{i}_{\text{m}}$ to obtain torques. Friction on the motors is denoted by $\boldsymbol{\tau}_{\text{fric}} \in \mathbb{R}^n$. The vector $\boldsymbol{\tau}_{\text{ext}} \in \mathbb{R}^n$ are the external joint torques, resulting from external forces and moments, summarized in the wrench vector $\boldsymbol{F}_{\text{ext}} = (f_x, f_y, f_z, m_x, m_y, m_z)^T$, that acts at the contact point $\boldsymbol{p}_{\text{c}} = \boldsymbol{k}(\boldsymbol{q}) \in \mathbb{R}^3$ on the robot. The relation between wrench and external joint torques is characterized by

$$\boldsymbol{\tau}_{\text{ext}} = \boldsymbol{J}_{\boldsymbol{p}_{\text{c}}}^T(\boldsymbol{q})\boldsymbol{F}_{\text{ext}}, \quad (2)$$

where $\boldsymbol{J}_{\boldsymbol{p}_{\text{c}}}(\boldsymbol{q}) \in \mathbb{R}^{6\times n}$ is the geometric Jacobian associated with a link frame at the contact point $\boldsymbol{p}_{\text{c}}$. For this work, it is essential to have well identified dynamic parameters, as well as a precise friction model. In the following, estimates of all dynamic terms are denoted by the hat symbol (). A more detailed explanation on the topic of dynamic model identification for robot manipulators can be found in [11] and [12].

B. Sensorless Collision Detection

We introduce two popular observers for the detection of an external force on the robot. The energy-based method, see [2], and the method based on the generalized momentum, see [7].

1) Energy-based Method: The first collision detection method is based on the system's energy. The key idea behind this method is that a collision will change the energy level of the system, and the residual energy $\sigma(t)$ will then be non-zero. In all other cases, it is always equal to zero, even if the robot is moving. According to [2], the residual energy of the system is defined as

$$\sigma(t) = k_{\text{o}}\left(\hat{T}(t) - \int_0^t (\dot{\boldsymbol{q}}^T(\boldsymbol{\tau}_{\text{m}} - \hat{\boldsymbol{g}}(\boldsymbol{q}) - \hat{\boldsymbol{\tau}}_{\text{fric}}) + \sigma)\mathrm{d}s - \hat{T}(0)\right) \quad (3)$$

where $\sigma(0) = 0$, $k_{\text{o}} > 0$ is a constant gain and $\hat{T}(t)$ is the estimation of the kinetic energy at time $t \geq 0$ defined as

$$\hat{T}(t) = \frac{1}{2}\dot{\boldsymbol{q}}^T\hat{\boldsymbol{M}}(\boldsymbol{q})\dot{\boldsymbol{q}}. \quad (4)$$

The method only relies on the available joint position $\boldsymbol{q}$, its filtered joint velocity $\dot{\boldsymbol{q}}$, and the measured motor torques $\boldsymbol{\tau}_{\text{m}}$. One can show that $\sigma(t) \approx \dot{\boldsymbol{q}}^{\text{T}}\boldsymbol{\tau}_{\text{ext}}$ for high filter gains and ideal conditions [2]. A drawback of this method is that no collisions can be detected when the robot is stationary.

2) Method based on the Generalized Momentum: The second approach followed in this work for the detection of a collision is based on the estimated generalized momentum

$$\boldsymbol{p} = \hat{\boldsymbol{M}}(\boldsymbol{q})\dot{\boldsymbol{q}} \quad (5)$$

of the robot. Based on (5), the momentum-based residual vector can be defined as follows [6]

$$\boldsymbol{r}(t) = \boldsymbol{K}_{\text{o}}\left(\boldsymbol{p}(t) - \int_0^t (\boldsymbol{\tau}_{\text{m}} - \hat{\boldsymbol{\beta}}(\boldsymbol{q},\dot{\boldsymbol{q}}) + \boldsymbol{r})\mathrm{d}s - \boldsymbol{p}(0)\right), \quad (6)$$

$$\hat{\boldsymbol{\beta}}(\boldsymbol{q},\dot{\boldsymbol{q}}) = \hat{\boldsymbol{g}}(\boldsymbol{q}) + \hat{\boldsymbol{C}}(\boldsymbol{q},\dot{\boldsymbol{q}})\dot{\boldsymbol{q}} - \hat{\dot{\boldsymbol{M}}}(\boldsymbol{q})\dot{\boldsymbol{q}} + \hat{\boldsymbol{\tau}}_{\text{fric}}. \quad (7)$$

The residuals are initialized with $\boldsymbol{r}(0) = \boldsymbol{0}$. The diagonal matrix $\boldsymbol{K}_{\text{o}} > \boldsymbol{0}$ contains the gains of the observer. The residuals $\boldsymbol{r}(t)$ can be computed solely based on the motor torques $\boldsymbol{\tau}_{\text{m}}$, the load-side encoder position $\boldsymbol{q}$ as well as its filtered velocity $\dot{\boldsymbol{q}}$. In [2], it is shown that for high filter gains the residual approximates the external torques

$$\boldsymbol{K}_{\text{o}} \to \infty \quad \Longrightarrow \quad \boldsymbol{r} \approx \boldsymbol{\tau}_{\text{ext}}. \quad (8)$$

Thus, ideally $\boldsymbol{K}_{\text{o}}$ is chosen as high as possible. However, in practice this also amplifies all unmodeled effects and the noise, which limits the choice of $\boldsymbol{K}_{\text{o}}$. The residual technique is theoretically able to detect collisions even when $\dot{\boldsymbol{q}} = \boldsymbol{0}$. In practice however, there are unmodeled effects, such as hysteresis effects in the drive train, or imperfect model knowledge, that lead to non-zero residuals. Therefore, thresholds for each residual are required to detect a contact robustly.

3) Combined Collision Detection: To reliably detect a collision, the energy-based and the momentum-based resid-

ual methods are combined. An outlier in any of the observer signals is only considered a collision if at least one of the components of $\boldsymbol{r}(t)$ and the energy-based residual $\sigma(t)$ exceed at the same time their time-varying thresholds.

III. SENSORLESS CONTACT POINT ISOLATION

The residual $\boldsymbol{r}(t)$ from (6) can be used as a virtual joint torque sensor. In the ideal case, if a contact occurs on link i, an external joint torque acts on joint i, such that $r_i \neq 0$. While there may be an external joint torque acting on any joint $l < i$, there are no external joint torques acting on all joints $l > i$, such that $r_{i+1} = ... = r_n = 0$. In this way, it is possible to isolate the link on which the contact occurs. Further, when the contact occurs at a link $i \geq 6$, it is possible to estimate the contact point $\boldsymbol{p}_{\mathrm{c},i}$ in link frame i without the need of any additional sensors [7]. In this work, no additional sensors are used other than the available encoder and current measurements. We combine two methods, the method based on the pseudoinversion applied in [7] and the CPF method from [9].

A. Contact Point Estimation via Pseudoinversion

The first approach is based on two pseudoinversions. First, the external joint torques $\boldsymbol{\tau}_{\text{ext}} \approx \boldsymbol{r}$, approximated by the residuals, are projected onto the frame of link i, where the contact is detected, by the pseudoinverse of the Jacobian of link i

$$\begin{pmatrix} \boldsymbol{f}_i \\ \boldsymbol{m}_i \end{pmatrix} = (\boldsymbol{J}_i^T(\boldsymbol{q}))^{\#}\boldsymbol{r}. \tag{9}$$

Here $\boldsymbol{f}_i$ and $\boldsymbol{m}_i$ are the estimates of the force and moments acting on link frame i due to the external joint torques. This projection suffers in the proximity of kinematic singularities, where even small residuals may cause a large contact wrench. Also, for a contact on any link $i < 6$, the Jacobian will not have full row rank and the pseudo-inversion suffers from the same numerical issues as in the presence of kinematic singularities. Following [7], we assume a contact where only contact forces and no moments ($\boldsymbol{m}_{\text{ext}} = \boldsymbol{0}$) occur, an assumption that is valid for most impulsive collision situations in practice. Thus, one can formulate the equilibrium of forces and moments around the origin of link frame i as follows

$$\begin{pmatrix} \boldsymbol{f}_i \\ \boldsymbol{m}_i \end{pmatrix} = \begin{pmatrix} \boldsymbol{I} \\ \boldsymbol{S}(\boldsymbol{p}_{\mathrm{c},i}) \end{pmatrix} \boldsymbol{f}_{\text{ext}}, \tag{10}$$

where $\boldsymbol{S}(\cdot)$ is a skew-symmetric matrix, that can be used to express the cross product between the contact point and contact force vectors, i.e., $\boldsymbol{p}_{\mathrm{c},i} \times \boldsymbol{f}_{\text{ext}} = \boldsymbol{S}(\boldsymbol{p}_{\mathrm{c},i})\boldsymbol{f}_{\text{ext}}$. From (10) one can see that $\boldsymbol{f}_i = \boldsymbol{f}_{\text{ext}}$. To get the contact point $\boldsymbol{p}_{\mathrm{c},i}$, the second row of (10) should be inverted, taking into account that the skew-symmetric matrix $\boldsymbol{S}$ is always singular with $\text{rank}(\boldsymbol{S}(\cdot)) = 2$. Thus, the solution space has dimension 1. The pseudoinversion provides the minimum norm solution for the contact point

$$\boldsymbol{p}_{\mathrm{c,d}} = (-\boldsymbol{S}(\boldsymbol{f}_{\text{ext}}))^{\#}\boldsymbol{m}_i. \tag{11}$$

The contact point $\boldsymbol{p}_{\mathrm{c,d}}$ found in this way is not constrained to lie on the surface of the link. However, the space of feasible solutions can be written in terms of a particular solution, e.g., (11), and a term in the null space of $\boldsymbol{S}^T(\boldsymbol{f}_{\text{ext}})$ as follows

$$\boldsymbol{p}(\lambda) = \boldsymbol{p}_{\mathrm{c,d}} + \lambda \frac{\boldsymbol{f}_{\text{ext}}}{||\boldsymbol{f}_{\text{ext}}||}, \quad \lambda \in \mathbb{R}. \tag{12}$$

By choosing the intersection between this *line of action* and the link surface, it is possible to estimate the contact point $\boldsymbol{p}_{\mathrm{c},i}$. In this work, we exploit the cylindrical shape of link 6, and choose the "pushing" solution in case two solutions exist. Further, we only consider solutions on the side of the cylindrical flange, not on the top.

B. Contact Point Particle Filter

We employ an adapted version of the contact particle filter presented in [9] and [13]. Instead of solving a quadratic program for the observation model, our work relies on a computationally simpler pseudoinversion, essentially combining the classical method described in Sec. III-A with the CPF. We only focus on link 6 of the robot due to the limitations of the least-squares method. However, it is easy to extend the method to any link $i > 6$.

Generally, a particle filter is a discrete, non-parametric Bayesian filter that can be applied to a variety of applications. It uses a set of discrete N samples, the *particles*, to approximate the posterior distribution of a system, and is thus not based on a specific parametric form like other filters [14].

Each particle $\boldsymbol{x}_t^{[m]}$, with $m = 1, ..., N$, is a hypothesis as to what the true state of the system, in this case, the contact point coordinates in link frame, may be at time t. The set of particles at time t is given as

$$\boldsymbol{\chi}_t = \left\{ \boldsymbol{x}_t^{[1]}, \boldsymbol{x}_t^{[2]}, ..., \boldsymbol{x}_t^{[N]} \right\}. \tag{13}$$

At each time step, all particles are propagated through a motion model that describes the expected system behaviour. The weight $w_t^{[m]}$ associated to particle m is then updated based on the observation of the system, i.e., the residuals $\boldsymbol{r}(t)$ in our case. Based on the weighted distribution of the old particles, a new set of particles is generated that has a larger likelihood to estimate the state correctly. The particle filter consists of several steps that are described in the following.

1) Initialization: Once a collision on link 6 is detected, the CPF is initialized. The initialization of the particles considers the estimated contact point $\boldsymbol{p}_{\mathrm{c},i}$ from the least-squares based algorithm described in Sec. III-A. The contact particles are initialized using a Gaussian multivariate distribution around $\boldsymbol{p}_{\mathrm{c},i}$. This locates the particles closer to the true contact point and avoids that the particle filter converges to an incorrect solution, e.g., a contact point with a pulling force on the opposite side of link 6 that would result in the same residuals. All particles are initialized to have equal weight. The initialization of the particles is visualized in Fig. 5(a).

2) Motion Model: The motion model describes the system dynamics, e.g., the probability of transition from one state to the subsequent state. This work uses a random walk model, similar to [13]

$$p(\boldsymbol{x}_t|\boldsymbol{x}_{t-1}) \propto \mathcal{N}(\boldsymbol{x}_t; \boldsymbol{x}_{t-1}, \boldsymbol{\Sigma}_{\text{motion}}), \tag{14}$$

where $\boldsymbol{\Sigma}_{\text{motion}}$ is the standard deviation of the normal distribution centered around $\boldsymbol{x}_{t-1}$. When a particle is propagated with this model, it results in a particle that is most likely no longer on the surface of the link, because the random motion is performed in all three Cartesian directions. For this reason, after the motion, the particle is projected back onto the nearest point on the link surface. However, to avoid projecting back the particles, polar coordinates can be used.

3) Measurement Model: The measurement or observation model captures the likelihood of the measurement $\boldsymbol{r}(t)$ assuming that particle $\boldsymbol{x}_t^{[m]}$ correctly describes the contact point coordinates. This can be expressed by the posterior probability $p(\boldsymbol{r}(t)|\boldsymbol{x}_t^{[m]})$. Based on this, the weight of each particle is updated. The measurements, in this case the residuals $\boldsymbol{r}(t)$, are a good, but noisy estimate of the external joint torques $\boldsymbol{\tau}_{\text{ext}}$. They can be assumed to follow a Gaussian model

$$\boldsymbol{r}(t) = \boldsymbol{\tau}_{\text{ext}} + \boldsymbol{\eta} \quad \text{with} \quad \boldsymbol{\eta} \sim \mathcal{N}(\mathbf{0}, \boldsymbol{\Sigma}_{\text{meas}}), \tag{15}$$

where $\boldsymbol{\Sigma}_{\text{meas}}$ is the standard deviation of the measurements. Following the line of ideas from [9], one can formulate an optimization problem that reflects how well the particle $\boldsymbol{x}_t^{[m]}$ can explain the measured residuals

$$\text{cost}(\boldsymbol{r}(t)|\boldsymbol{x}_t^{[m]}) = \min_{\boldsymbol{f}_{\text{ext}}} \|(\boldsymbol{r}(t) - \boldsymbol{J}_{\text{c}}^{\text{T}}(\boldsymbol{q}, \boldsymbol{x}_t^{[m]})\boldsymbol{f}_{\text{ext}})\|_{\boldsymbol{\Sigma}_{\text{meas}}^{-1}}. \tag{16}$$

This optimization problem is solved for each particle at every time step. Since the contact point is fixed for each particle, this optimization problem is quadratic and convex, and thus easy to solve. Also, compared to the formulation of [9], we remove the friction cone constraint on the external force, since this constraint has not shown significant influence on our results. On the contrary, the removal of the constraints allows the usage of the weighted pseudo-inverse to solve (16) in a computationally more efficient manner

$$\boldsymbol{f}_{\text{ext}} = (\boldsymbol{J}_{\text{c}}^T(\boldsymbol{q}, \boldsymbol{x}_t^{[m]}))^{\#}_{\boldsymbol{\Sigma}_{\text{meas}}^{-1}} \boldsymbol{r}(t). \tag{17}$$

Thus, the importance weight can be updated based on

$$p(\boldsymbol{r}(t)|\boldsymbol{x}_t^{[m]}) \propto e^{-\frac{1}{2}\text{cost}\left(\boldsymbol{r}(t)|\boldsymbol{x}_t^{[m]}\right)}. \tag{18}$$

This has to be done for all N particles in every time step.

4) Importance Sampling: After the propagation of the samples through the dynamical model and the updating of the weights as a measure of the quality of each particle, a new set of particles $\boldsymbol{\chi}_t$ is generated based on the old set $\bar{\boldsymbol{\chi}}_t$. The underlying idea is to draw a new set of particles based on the cumulative distribution of the old data set, where the importance weights equal the probability of drawing each particle from the old distribution. This will change the distribution of the new particles, favouring the generation of particles that resemble the best particles of the old set. The estimated external force $\boldsymbol{f}_{\text{ext}}$ and contact point $\boldsymbol{p}_{\text{c},i}$ are computed by a weighted sum of all particles and associated forces. The contact particle filter is summarized in Algorithm 1.

Algorithm 1 Contact_Particle_Filter $(\boldsymbol{\chi}_{t-1}, \boldsymbol{r}(t))$

```
if χ_{t-1} = ∅ then
    χ_{t-1} = χ_init
    w_t = w_init
else
    χ̄_t = ∅
    for m = 1, 2, ..., N do
        sample x_t^[m] ~ p(x_t | x_{t-1}^[m])
        w_t^[m] ~ p(r(t)|x_t^[m]) ∝ e^{-1/2 cost(r(t)|x_t^[m])}
        χ̄_t = χ̄_t + < x_t^[m], w_t^[m] >
    end for
    χ_t = Importance_Sampling(χ̄_t)
end if
return χ_t
```

IV. EXPERIMENTS

In this section we realize the proposed collision detection, isolation and identification pipeline and validate our proposed approach in a set of three experiments. First, we show the experimental validation of a combination of the energy-based and the generalized momentum-based collision detection algorithm. The contact forces are then measured using an external sensor. Last, we compare the classical method for the contact point estimation from Sec. III-A with our proposed, adapted CPF implementation experimentally.

A. Experimental Setup

Figure 1 shows the experimental setup of LARA 5, a 6-axis cobot by NEURA Robotics. The robot uses strain-wave gear boxes and achieves a maximum joint velocity of $180°$/s and a maximum end-effector velocity of 3 m/s. The singularities of an anthropomorphic arm with a spherical wrist are described in detail in [15]. The high-level control software runs at a rate of 1000 Hz. LARA 5 is equipped with 24-bit dual encoders on each joint. For the estimation of the motor torques $\boldsymbol{\tau}_{\text{m}}$, only the motor current measurements are available, such that $\boldsymbol{\tau}_{\text{m}} = \boldsymbol{K}_{\text{i}}\boldsymbol{i}_{\text{m}}$. Experiments were conducted in the laboratory facilities of NEURA Robotics GmbH.

B. Experimental Results for Collision Detection

First, we show two experiments that combine the energy-based and the generalized momentum-based methods for collision detection. By combining the two methods, we are able to reduce the number of false positives making use of the advantages of both approaches.

1) Robust Collision Detection: The first testing scenario is designed to show the robustness of our combined approach. Up to $t = 2.5$ s, the robot is stationary and then executes a point-to-point motion with a maximum end-effector velocity of 250 mm/s during which link 3 collides with a human arm. Figure 2 shows the residuals during the trajectory for both the energy-based and the generalized momentum-based methods. At the beginning of the trajectory, there are spikes in the residual r_1 of the generalized momentum, although there was no collision. These spikes possibly result from

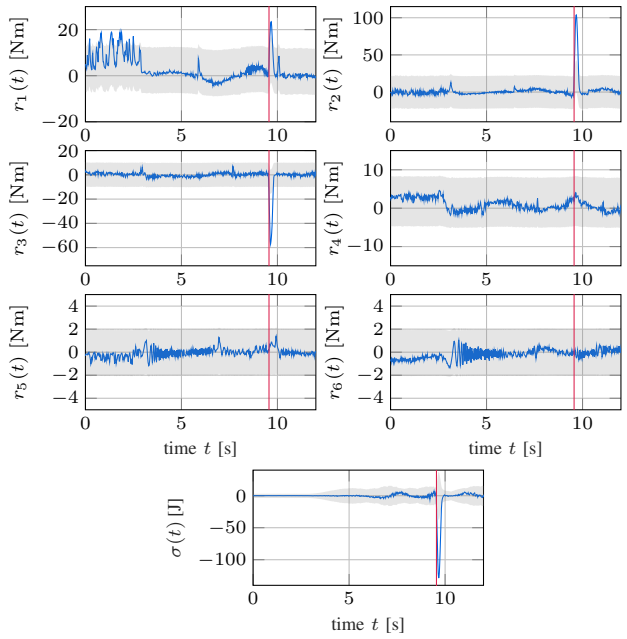

Fig. 2: Residuals of the generalized momentum-based and the energy-based method. The grey areas show the threshold tubes for each residual. The red vertical line marks the detected collision during the motion.

Fig. 3: Experimental setup of LARA 5 colliding with a GTE CoboSafe sensor.

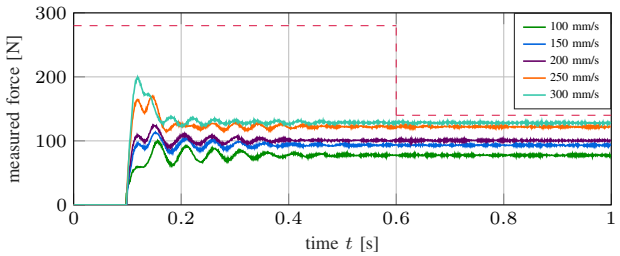

Fig. 4: Measurements of the realized contact forces using the GTE CoboSafe sensor for different end-effector velocities. In each of the phases of the contact, the measured contact forces lie below the maximum allowed limit force (- -) according to ISO 10218.

unmodeled effects, like static friction or hysteresis effects. Since the residual of the energy-based method is driven by the work performed by the external torque $\sigma(t) \approx \dot{\boldsymbol{q}}^{\mathrm{T}}\boldsymbol{\tau}_{\mathrm{ext}}$, it is more difficult to excite it when the joint velocities are low. From a safety point of view, collisions with a stationary robot, however, are unproblematic.

At $t = 9.56\,\mathrm{s}$ of the trajectory, the moving robot collides with a human arm. Both methods exceed their respective thresholds at the same time and a collision is detected. In the shown example, the residual of the generalized momentum of link 3 shows a spike, from which one can conclude that the contact occurs indeed on link 3. Different types of trajectories with varying velocities have been tested in this work, yielding similarly robust results. Combining both methods allows thus to robustly detect collisions during the motion of the robot, and eliminates the number of false positives, e.g., at the beginning of a trajectory.

2) Maximum Contact Force Validation: In order to validate the contact force at which a collision is detected, we are using the CoboSafe-CBSF-75 sensor by GTE Industrieelektronik. This device is a force-pressure measuring system that is specifically designed to measure the quasi-static and transient contact forces in pHRI [16]. The experimental setup can be seen in Fig. 3. The scenario is designed to simulate a pick and place application where the robot collides with a stationary, rigid object, located approximately $0.78\,\mathrm{m}$ from the robot's base. The experiment is repeated for different velocities that are representative for typical pHRI scenarios. Figure 4 shows the measured contact forces using the CoboSafe-CBSF-75 sensor, as well as the permitted collision forces for a human hand. The contact force is separated into two regions: First the transient phase, that describes the time between beginning of the contact until $0.5\,\mathrm{s}$ after the beginning of the contact, which is when the static phase of the collision starts. As can be seen from Fig. 4, the proposed collision detection method fulfills the requirements regarding the maximum allowed contact forces for the described scenario according to ISO 10218.

C. Contact Point Isolation

Finally, we experimentally validate our adapted CPF for the contact point estimation and compare our results with the results obtained with the pseudoinverse based method from Sec. III-A. In the experiment, the robot executes a point-to-point motion while we press against link 6 in the positive y-direction. The CPF runs at a rate of 50 ms, while $N = 150$ particles are being used. The distribution of the particles at different times during the experiment and the estimated contact force direction are shown in Fig. 5. Figure 6 shows the residuals $\boldsymbol{r}(t)$, as well as the estimated contact point and the contact forces for both methods during the trajectory. Since we do not use any additional sensor, the true contact force is unknown. One can see, however, that both methods show similar estimates for the contact forces. Regarding the estimated contact point, one can state that the suggested CPF scheme yields more robust results than the classical pseudo-inverse method. While the pseudoinverse method shows an error of 10 cm with the contact point no longer lying on the link cylinder, our adapted CPF has an error of only 2.5 cm. When comparing our work to the results

(a) particle initialization ($t = 1.7$ s, 0 iterations)

(b) particle convergence ($t = 2.0$ s, 6 iterations)

(c) particles at end of trajectory ($t = 11.0$ s, 186 iterations)

Fig. 5: Experimental results of the proposed CPF approach. Contact particles are shown in red at three different time instants. The green point is the ground truth contact point, the blue arrow indicates the estimated force applied at the estimated contact point. The three time instants of the experiment are marked with (a), (b), and (c) in Fig. 6.

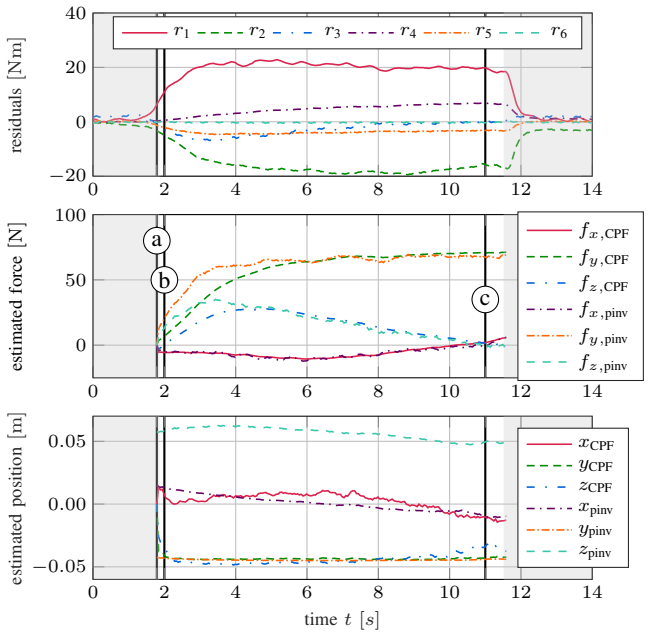

Fig. 6: Estimated residuals $\boldsymbol{r}(t)$, and estimated contact position $\boldsymbol{p}_{\text{c},i}$ and force $\boldsymbol{f}_{\text{ext}}$ in the frame of link 6 during the experiment for the CPF and the classical method. The contact is located at $\boldsymbol{p}_{\text{c,true}} = (0, -0.04, -0.025)^T$ m in link 6 frame. The grey areas show the times where no collision is detected and the CPF is not running.

presented in the literature, we can state that we achieve a comparable accuracy. In [10], a CPF is applied on a KUKA LBR iiwa experimentally, where a contact point accuracy below 2 cm is achieved on link 6, using 10000 particles.

D. Discussion

1) Model Accuracy: In theory, after a short transient, the residuals $\boldsymbol{r}(t)$ of the generalized momentum method equal the external joint torques $\boldsymbol{\tau}_{\text{ext}}$. However, this only holds when model and physical robot match each other. All methods used in this work rely only on motor current and joint encoder measurements. Motor current measurements are typically much more influenced by friction, hysteresis and temperature effects compared to joint torque sensors. This stresses the need to have a well identified friction and dynamical model of the robot. Any model discrepancies or unmodeled effects will result in large residuals, and consequently inaccurately identified collisions, contact forces and points. At stationary configurations, static friction and hysteresis effects are dominant and large residuals were found in our experiments. Therefore, we excluded stationary cases from our work, considering only dynamic situations. These are anyway more relevant for safety evaluation in pHRI.

2) Limitations: Apart from the just mentioned restriction, there are other limitations of our approach. Since we use the pseudoinversion of the Jacobian, see (9), the contact force estimation suffers from numerical issues for links $i < 6$ and in the proximity of kinematic singularities. As described earlier, in both cases, the Jacobian will not have full rank, and the obtained contact forces from the pseudoinversion will only be a poor estimate.

V. CONCLUSION

In summary, this paper shows the experimental validation of a contact detection, isolation and reaction scenario on a LARA 5 cobot. First, we combine the energy-based and the generalized momentum-based methods to reliably detect a contact and to reduce the number of false positives. The experiments are conducted using only motor current and joint encoder readings and are verified using an external GTE CoboSafe measurement system. For the contact point isolation, both the classical method relying on the inversion of the contact Jacobian, and an adapted contact particle filter are used to isolate the contact point. Here, our proposed contact particle filter outperforms the classical method. Both methods are based on the residuals of the generalized momentum to estimate the external joint torques. We have shown for the first time the application of the contact point estimation without relying on joint torque sensors. This eliminates the need for expensive hardware.

REFERENCES

[1] F. Flacco, T. Kröger, A. De Luca, and O. Khatib, "A depth space approach to human-robot collision avoidance," in *Proc. IEEE Int. Conf. on Robotics and Automation*, 2012, pp. 338–345.

[2] S. Haddadin, A. De Luca, and A. Albu-Schäffer, "Robot collisions: A survey on detection, isolation, and identification," *IEEE Trans. on Robotics*, vol. 33, no. 6, pp. 1292–.1312, 2017.

[3] D. P. Le, J. Choi, and S. Kang, "External force estimation using joint torque sensors and its application to impedance control of a robot manipulator," in *Proc. 13th Int. Conf. on Control, Automation and Systems*, 2013, p. 1794–1798.

[4] R. S. Dahiya, P. Mittendorfer, M. Valle, G. Cheng, and V. J. Lumelsky, "Directions toward effective utilization of tactile skin: A review," *IEEE Sensors J.*, vol. 13, no. 11, pp. 4121–4138, 2013.

[5] A. De Luca and R. Mattone, "Sensorless robot collision detection and hybrid force/motion control," in *Proc. IEEE Int. Conf. on Robotics and Automation*, 2005, pp. 999–1004.

[6] A. De Luca, A. Albu-Schäffer, S. Haddadin, and G. Hirzinger, "Collision detection and safe reaction with the DLR-III lightweight manipulator arm," in *Proc. IEEE/RSJ Int. Conf. on Intelligent Robots and Systems*, 2006, pp. 1623–1630.

[7] G. Buondonno and A. De Luca, "Combining real and virtual sensors for measuring interaction forces and moments acting on a robot," in *Proc. IEEE/RSJ Int. Conf. on Intelligent Robots and Systems*, 2016, pp. 794–800.

[8] M. Iskandar, O. Eiberger, A. Albu-Schäffer, A. De Luca, and A. Dietrich, "Collision detection, identification, and localization on the DLR SARA robot with sensing redundancy," in *Proc. IEEE Int. Conf. on Robotics and Automation*, 2021, pp. 3111–3117.

[9] L. Manuelli and R. Tedrake, "Localizing external contact using proprioceptive sensors: The Contact Particle Filter," in *Proc. IEEE/RSJ Int. Conf. on Intelligent Robots and Systems*, 2016, pp. 5062–5069.

[10] J. Bimbo, C. Pacchierotti, N. G. Tsagarakis, and D. Prattichizzo, "Collision detection and isolation on a robot using joint torque sensing," in *Proc. IEEE/RSJ Int. Conf. on Intelligent Robots and Systems*, 2019, pp. 7604–7609.

[11] J. Swevers, W. Verdonck, and J. De Schutter, "Dynamic model identification for industrial robots," *IEEE Control Systems Mag.*, vol. 27, no. 5, pp. 58–71, 2007.

[12] J. Hollerbach, W. Khalil, and M. Gautier, "Model identification," in *Springer Handbook of Robotics*, B. Siciliano and O. Khatib, Eds. Cham: Springer, 2016, pp. 113–138.

[13] L. Manuelli, "Localizing external contact using proprioceptive sensors: The contact particle filter," Master's thesis, Massachusetts Institute of Technology, 2018. [Online]. Available: https://youtu.be/pnQkkxWKXNk

[14] S. Thrun, W. Burgard, and D. Fox, *Probabilistic Robotics*. Cambridge, Mass.: MIT Press, 2005.

[15] B. Siciliano, L. Sciavicco, L. Villani, and G. Oriolo, *Robotics: Modelling, Planning and Control*. Springer, 2009.

[16] P. Svarny, J. Rozlivek, L. Rustler, and M. Hoffmann, "3D collision-force-map for safe human-robot collaboration," in *Proc. IEEE Int. Conf. on Robotics and Automation*, 2021, pp. 3829–3835.